To be submitted to
Nucl. Instr. & Meth.

ISTITUTO NAZIONALE DI FISICA NUCLEARE
Laboratori Nazionali di Frascati

LNF-85/48(P)
24 Ottobre 1985

G. Battistoni, E. Bellotti, C. Bloise, G. Bologna, P. Campana, C. Castagnoli, V. Chiarella, O. Cremonesi, D. Cundy, B. D'Ettorre Piazzoli, E. Fiorini, E. Iarocci, G. Mannocchi, G.P. Murtas, P. Negri, G. Nicoletti, P. Picchi, M. Price, A. Pullia, S. Ragazzi, M. Rollier, F. Ronga, O. Saavedra, and L. Zanotti:

THE NUSEX DETECTOR

Servizio Documentazione
dei Laboratori Nazionali di Frascati
Cas. Postale 13 - Frascati (Roma)

INFN - Laboratori Nazionali di Frascati
Servizio Documentazione

LNF-85/48(P)
24 Ottobre 1985

THE NUSEX DETECTOR

G. Battistoni[a], E. Bellotti[b] ,C. Bloise[a], G. Bologna[c], P. Campana[a], C. Castagnoli[c], V. Chiarella[a], O. Cremonesi[b], D. Cundy[d], B. D'Ettorre Piazzoli[c], E. Fiorini[b], E. Iarocci[a], G. Mannocchi[c], G.P. Murtas[a], P. Negri[b], G. Nicoletti[a], P. Picchi[c], M. Price[d], A. Pullia[b], S. Ragazzi[b], M. Rollier[b], F. Ronga[a], O. Saavedra[c], and L. Zanotti[b].

[a] INFN - Laboratori Nazionali di Frascati, Frascati (Italy)
[b] Dipartimento di Fisica dell'Università and INFN - Sezione di Milano, Milano (Italy)
[c] Istituto di Cosmogeofisica del CNR, Torino (Italy)
[d] CERN, European Organization for Nuclear Research, Geneva (Switzerland)

ABSTRACT

We present in this paper the characteristics, trigger system and performance of the NUSEX detector, designed to study nucleon stability, running in the Mt. Blanc laboratory.

1. - INTRODUCTION

In recent years theoretical predictions on baryon number non conservation and proton or bound neutron lifetime in the range 10^{30}–10^{32} [1] years have raised interest in building detectors dedicated to the study of nucleon decay.

The main characteristics of a detector capable of reaching significant results can be briefly summarized as: (a) large number of nucleons ($\gtrsim 10^{32}$) under observation; (b) high rejection capability against background events, i.e. events due to cosmic muons, neutrons, or atmospheric neutrinos.

In order to fulfill these requirements massive apparata acting both as possible source and as detector of nucleon decay have been built [2]. The detectors are placed deep underground in order to reduce at a negligible level cosmic rays and neutron background, and in many cases an outer shell of the detector itself acts as an anticoincidence against incoming particles.

This is not the case for the background of atmospheric neutrinos which produce events originating inside the detector with no detectable correlations with anything external; they can thus fake nucleon decay events. Since the estimated [3], and now measured [4] neutrino interaction rate is about 150 events/(kton×year), above a threshold of about 250 MeV of visible energy. The nucleon lifetime limit achievable by an experiment with no neutrino rejection capability would thus be of the order of 4×10^{30} years.

Neutrino background rejection can be achieved with energy and topology cuts on the events. An unambiguos interpretation of the events is required in order to prove the nucleon decay. Both good energy resolution and event reconstruction capability are therefore necessary for a nucleon decay experiment. In order to reach these goals we have built a fine grain calorimeter.

The NUSEX detector, running since June 1982, was intended to be sensitive to a nucleon lifetime $\simeq 10^{31}$ years, designed to be installed inside an existing underground laboratory. In this paper we present its characteristics and discuss its performance.

2. - THE LABORATORY

The detector is installed in the Garage 17 in the road tunnel under the Mont Blanc at 45.8° N latitude and 6.9 ° E longitude, 42.7° geomagnetic latitude. The shape of the rock overburden, as a function of the azimuthal angle ϕ and of the zenithal angle θ referred to the detector vertical, is shown in Fig. 1.

It can be seen that rock thickness exceeds 4800 m.w.e. (metres of water equivalent) in every direction. Fig. 2 shows the general lay-out of the laboratory. It is divided into two rooms. An air conditioning system, gas system and power backup system are placed in the front room. The detector, readout and trigger electronics, low voltage and high voltage supplies, and the computer are placed in the next room. Free space is left beside the detector for assembly purposes.

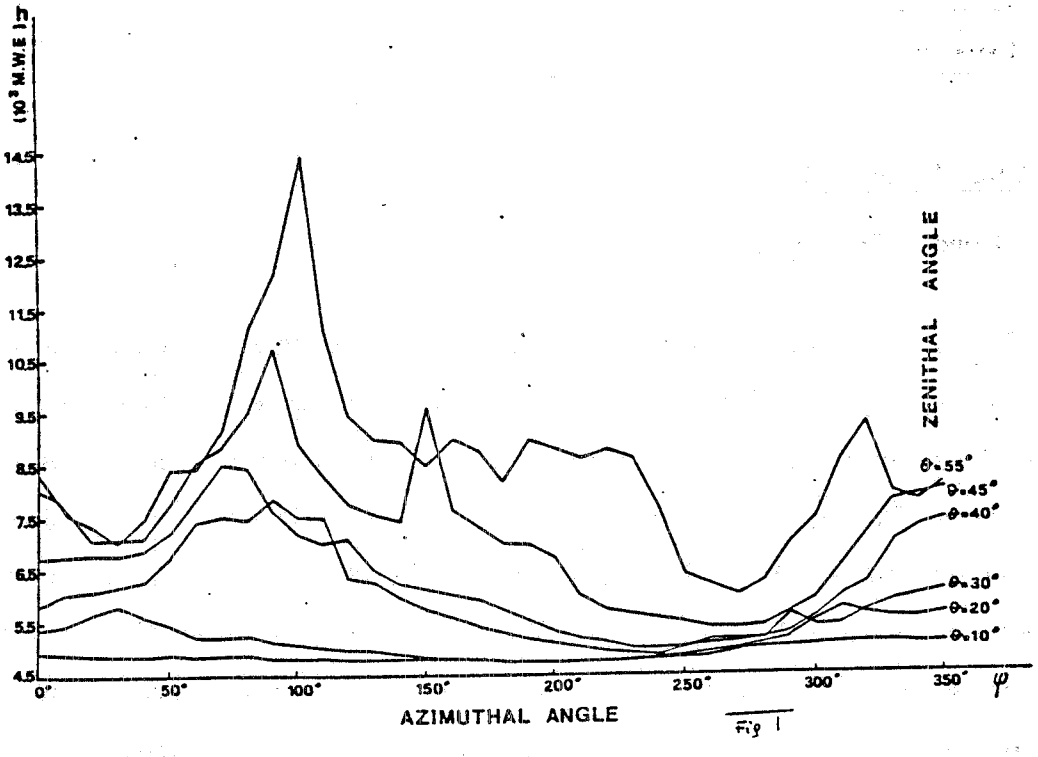

FIG. 1 - Slant depth in hg·cm^{-2} (meters of water equivalent) as a function of θ and Ø at the Mont Blanc Laboratory.

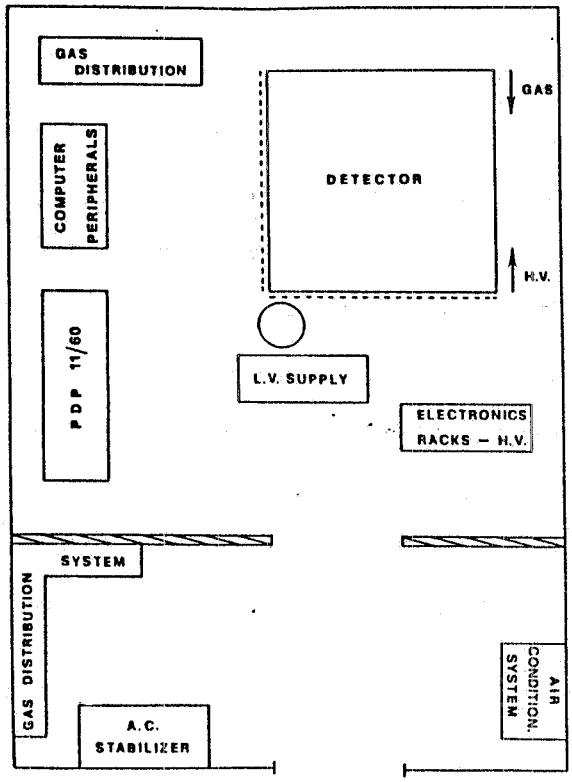

FIG. 2 - Layout of the Mont Blanc Laboratory.

3. - THE DETECTOR

3.1. - General Description

The detector is a digital tracking calorimeter, consiting of a sandwich of 134 horizontal iron plates 3.5 m × 3.5 m × 1 cm thick, interleaved with plastic streamer tubes 3.5 m long and 9x9 mm^2 in cross section. One detector plane contains 320 such tubes. The gap between two iron plates is 1.7 cm. Detector height is 368 cm, and the total mass is 150 tons, with an average density 3.5 g/cm^3. A sketch of the detector is shown in Fig. 3. Detector size and its location inside the laboratory were chosen in order to allow easy mounting and possible replacement of modules.

Iron was chosen for its low cost, good mechanical characteristics and principally because maximum detector density can be reached, while conserving a good sampling for showers energy measurement and track reconstruction. A detector of the same average density built with Pb plates would have a sampling of $1.2X_0$ instead of $0.57\ X_0$ for Fe, while a low density detector not only implies a lower mass when room is limited but also a lower fiducial volume for equal masses.)

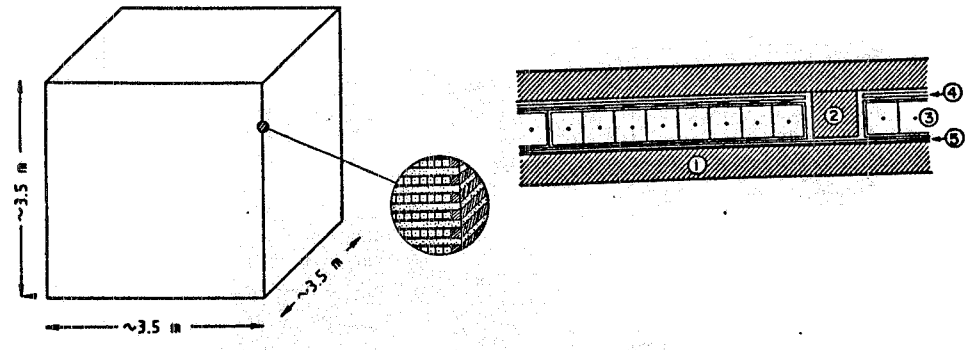

FIG. 3 - a) Sketch of the Nusex detector. b) a detector plane: 1) iron plate; 2) iron spacer; 3) streamer tube; 4) X-strips; 5) Y-strips.

3.2. - The Streamer Tubes

The tubes have a modular structure consisting of chambers containing 16 individual tubes. A tube chamber, 3.5 m long, is composed by two constructive units, each containing 8 wires. Details of a tube chamber are shown in Fig. 4. The basic element is an open 8-tube profile, extruded in PVC. The single cell is 9×9 mm^2, and the wire diameter is 100 μm. The tube walls are coated with graphite ($R \geq 50$ kΩ/ square) to perform the cathode function. Plastic holders support the wire every 50 cm, thus avoiding electromechanical instabilities and handling problems. The wires of each unit are soldered at both ends on printed circuit boards, where they are connected to a common high voltage. This 8-tube profile is closed by a PVC top cover, .5 mm thick, also coated with graphite ($R \geq 100$ kΩ/square). Two of such 8-tube units are inserted into a PVC extruded envelope, which acts as gas container. The H.V. connection and the ground connection to the graphite are located on one of the two end caps which close the 16-tube module. Gas distribution is through connectors on the same end-cap.

Each plane of the apparatus consists of 20 contiguous 16-tube chambers. The total number of tubes is 42880.

As shown in Fig. 5, the tube planes are equipped with X and Y pick-up strips for two dimensional localization. Both sets of strips are made of 40 μm thick aluminum strips on one side of a PVC sheet. A 40 μm aluminum sheet is attached

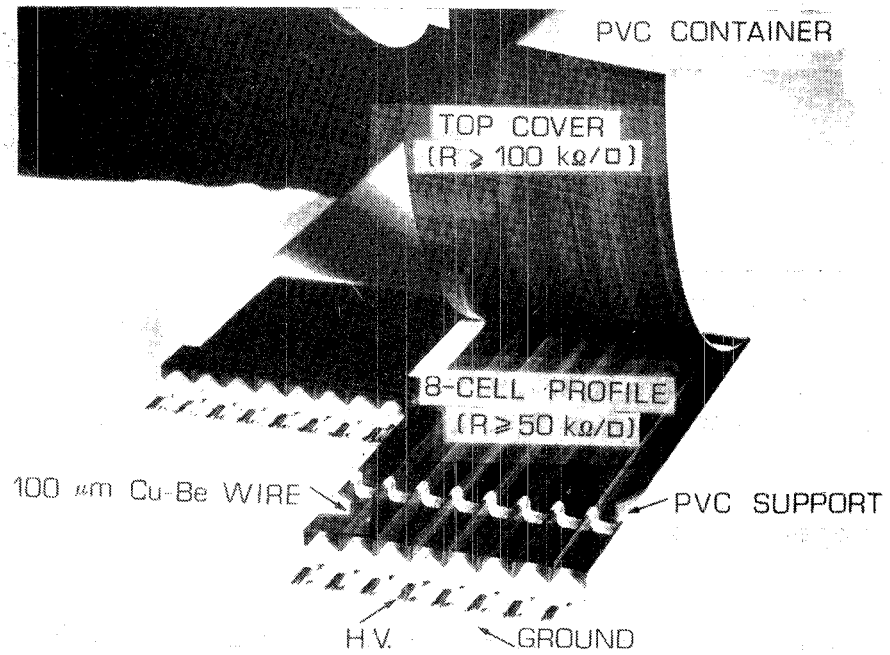

FIG. 4 - Details of the streamer tubes.

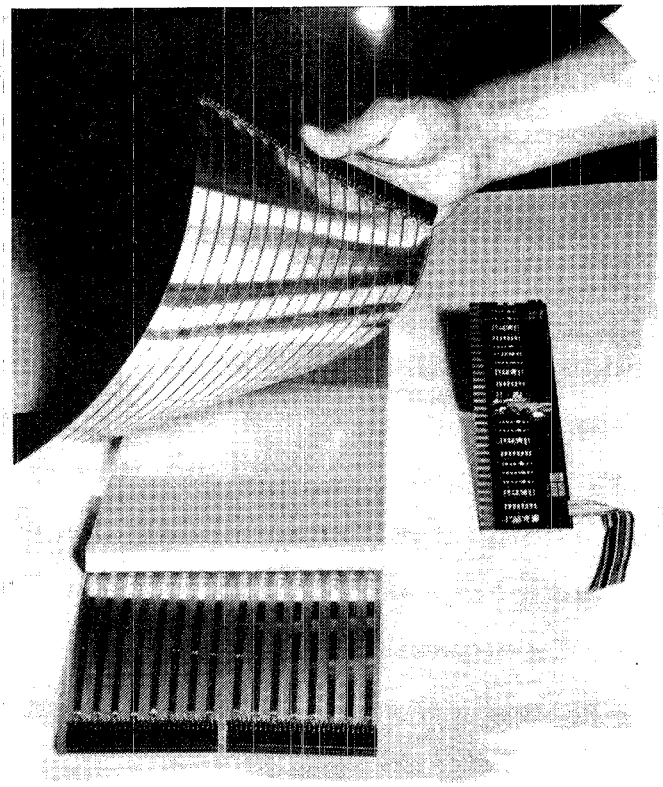

FIG. 5 - Pick-up strips and readout card for the streamer tubes: Xstrips are 4 mm wide with 1 cm pitch. Y-strips are 10 mm wide with 1.2 cm pitch.

to the other side of the PVC sheet, and serves as the ground electrode and shield. The pick-up strips behave as transmission lines [5] with characteristic propagation time $\sim$ 6 ns/m, and characteristic impedance $\sim$ 50 Ω for the X strips and $\sim$ 25 Ω for the Y strips. The total number of strips (X+Y) is 81472.

The H.V. is distributed to the tube modules by means of one bus every two planes. A 50 MΩ limiting resistor is used for each 8-tube unit.

The gas mixture is Ar + CO_2 + n-Pentane (1+2+1), obtained by flowing an Ar + CO_2 mixture in liquid n-Pentane kept at 10° C. The gas is distributed by means of 134 flow lines (one for each tube plane); the tube modules of one plane are connected in series. The flow rate is $\sim$ 0.3 detector volumes/day.

Fig. 6 shows the singles counting rate as a function of high voltage, for a β source, as measured on a tube module. The plateau of this curve corresponds to the full efficiency region [6]. The working point has been chosen just above the knee of the plateau (3.9 kV). Fig. 7 shows the wire and strip pulses at the operation voltage.

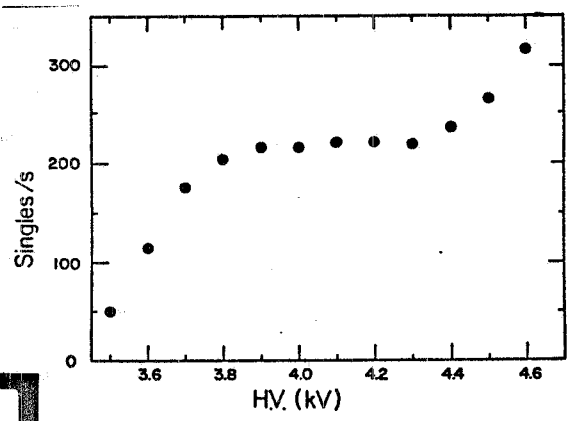

FIG. 6 - Singles rate counts as a function of high voltage.

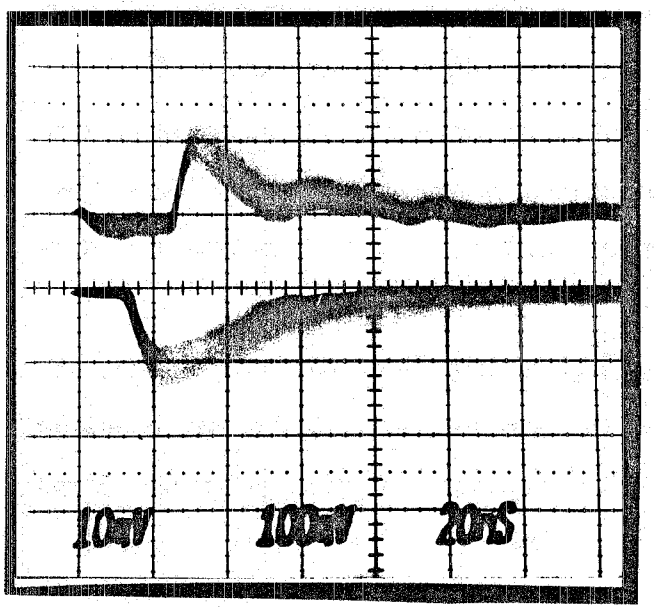

FIG. 7 - Strip and wire pulses at 3.9 kV.

3.3. - The Readout chain

Signals from strips are fed into a monolithic dual channel comparator-one-shot circuits (Le Croy MIL200—threshold $\sim$ 2 mV/50 Ω). The output pulses are shaped to 7 μs in order to allow delayed readout. Outputs from 8 contiguous channels are then fed into an 8-bit parallel-in serial-out shift register. The strips are directly connected to the readout cards, each one containing 32 channels (LeCroy 4200). A single bus allows serial readout of all the shift registers of each plane (both X and Y strips). A single CAMAC processor Seventeen processors are then required to operate the whole detector. A trigger to the processor loads the signals to the shift registers and starts the serial shift of data from the cards to the controller which encodes in 16-bit words the position and size of clusters (up to eight contiguous channels hit) and loads the data into a FIFO memory 40 words deep. A 'clear' to the processor can be sent to stop the conversion and clear its contents. Fast-OR signals are provided for each plane, and are fed to a group of single-in–fan-out units which provide NIM and TTL outputs shaped to 2 μs both for individual planes and for groups of 8 contiguous planes OR-ed together. The ORs from individual planes, delayed by 1 μs, are used as stop signals for a set of 134 TDCs which record the arrival time of the OR of each plane with 100 ns time resolution. The ORs from groups of 8 planes are used to load FIFO memories of a set of 16 TDCs with 1 μs resolution, used, as will be described in section 3.4.2, to record information on 'monopole triggers'. The scheme of the time recording logic is shown in fig. 8.

When the trigger system detects a good event a trigger is sent to the processors, after which standard CAMAC readout and clear of processors and TDCs is started. A clock providing absolute time information with an error of $\sim$ 1 ms is also readout at each trigger.

The length of an event due to a single μ crossing the whole detector is typically 500–600 16-bit words. Data acquisition is controlled by a PDP 11/60 computer CAMAC interfaced to the system. Dead time after a trigger is $\sim$ 10 ms. Event information is stored on magnetic tape and disk.

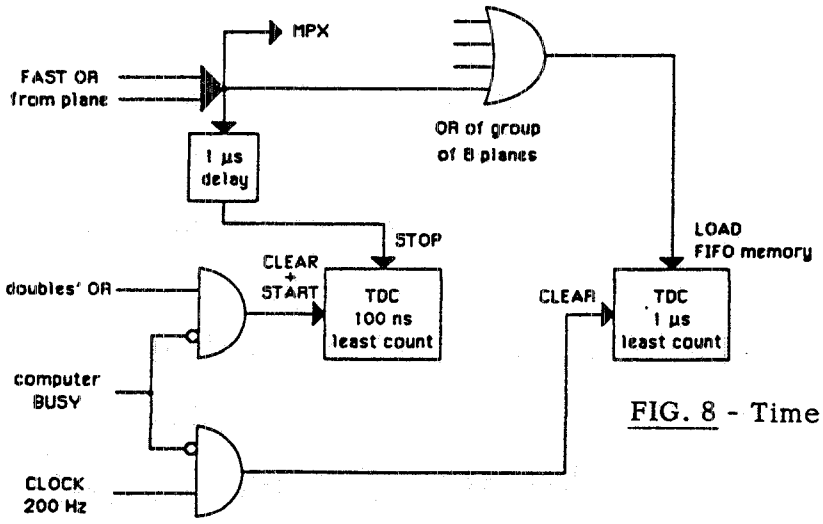

FIG. 8 - Time recording logic.

3.4. - The Trigger system

Two idependent logic chains are used to trigger the NUSEX detector.Both of them are built starting from the fast-ORs of planes. The first trigger chain operates on prompt coincidences between planes (hereafter it will be called 'main trigger'); the second logic chain, designed to be sensitive to slowly moving penetrating particles (e.g. magnetic monopoles), operates on delayed coincidences between groups of planes (we shall call it 'monopole trigger').

The OR rates of planes range from 2.5 kHz on the topmost plane (plane 1) down to $\approx$ 300 Hz on the inner planes (planes 20–128), raising again to 800 Hz on plane 136. Counts on the inner planes are mainly due to radioactivity of ^{60}Co contained in the iron, while counts on outer planes are due to radioactivity of rock and concrete. The higher radioactivity of the rock of the ceiling with respect to the concrete of the floor accounts for the up-down asymmetry.

3.4.1. - The main Trigger

The requirements which are to be fulfilled by the main trigger are a high detection efficiency for cosmic muons, atmospheric neutrinos and nucleon decay events, together with a reasonably low counting rate. Its logic has been designed in such a way as to generate a trigger whenever one of the following patterns is found in the detector :

a) at least 4 contiguous planes hit, or

b) 3 contiguous planes plus at least 2 contiguous planes, or

c) at least 3 separated pairs of contiguous planes.

The resulting frequency is 7 triggers/hour. Trigger performance will be discussed later.

The 'main trigger' logic is shown in fig. 9; details of the logic are explained in appendix A.

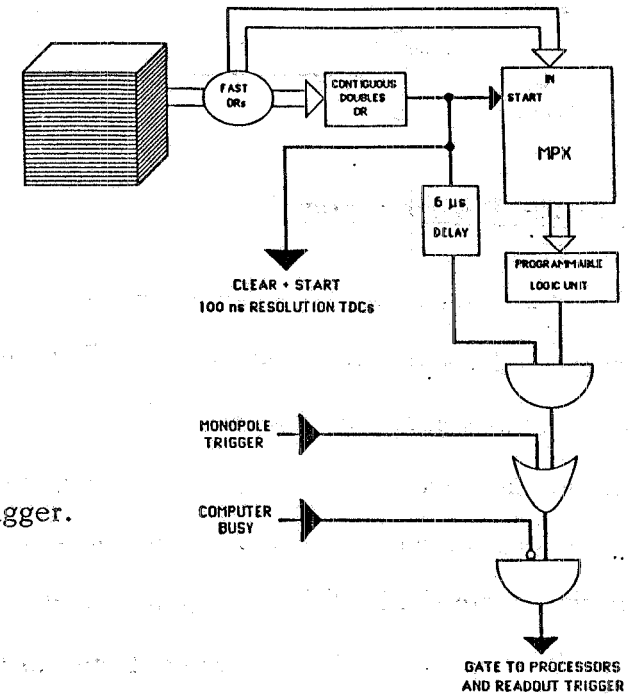

FIG. 9 - Sketch of the main trigger.

3.4.2. - The monopole Trigger

This trigger system, installed after 10 months of detector operation and upgraded 1 year later, has been designed in order to detect slowly moving, low ionizing penetrating particles. In designing it we had to take into account that, in the gas mixture used in NUSEX, a minimum ionizing particle produces 30–50 primary electrons per cm, which in turn generate a total of about 150 ion pairs. The detection efficiency for a single ion pair is $\simeq$10% [7], therefore the single tube detection efficiency is near to 100% for an ionization $I \gtrsim 10^{-1} I_{min}$ (where I_{min} is the ionization produced by a particle at minimum). The main trigger, as explained before, requires 4 planes hit within 2.0 μs , then it is sensitive to particles with a velocity

$\beta > 4 \times 10^{-4}$ and $I \gtrsim 10^{-1} I_{min}$. Moreover the trigger delayed by 5 μs with respect to the triggering pattern allows recording of space or time information only for hits occuring within a 5 μs window; therefore it allows recording of space or time information for all hits produced by a particle crossing the whole detector only if $\beta \gtrsim 2 \times 10^{-3}$.

In recent years many calculations have been done concerning the ionization of slowly moving magnetic monopoles [8]. While everybody agrees that for $\beta > 10^{-3}$ I is greater than I_{min}, the situation is not clear for $10^{-4} < \beta < 10^{-3}$. In this range in fact the ionization rapidly falls below I_{min}, but the excitation of atomic levels of noble gases followed by the Penning effect could become a relevant process. Therefore it seemed reasonable to design a trigger system with a β threshold near to 10^{-4} (escape velocity from the solar system) and sensitive to ionizations $I \gtrsim 10^{-2} I_{min}$.

In order to obtain a reasonably high detection efficiency, even at low ionizations, for each element entering in the logic, planes were then ORed together in 16 groups of eight (we use planes 1–128 only). Two consecutive groups, except 1 and 2, are in turn ORed together to form the elements of a 9-fold delayed coincidence used to trigger the data acquisition. The arrival time of hits on each group of eight planes is recorded by a 1 μs resolution TDC with FIFO memory. The basic scheme of the trigger for donward going monopoles is shown in Fig. 10. A similar logic is used for an upward going monopole; details of the logic are explained in appendix B.

This trigger system is sensitive to particles crossing the detector in a time $t < 120$ μs, corresponding to a velocity $\beta > 10^{-4}$. However the digital readout memory ~ 7 μs, therefore this system does not allow all hits involved in a trigger to be visualized. A monopole candidate is then obtained when the vertical coordinates (Z) of hits, known by means of TDCs with an incertitude of 8 planes, plotted versus times (known with an error of ± 0.5 μs) fit a straight line.

In order to obtain a more restrictive condition on monopole candidates , in April '84 the visualization of hits (i.e. recording of full space information) has been introduced. This is obtained using , after a 5 μs delay, the same signal which is input to a TDC as a trigger to the processor controlling the corresponding 8 planes.

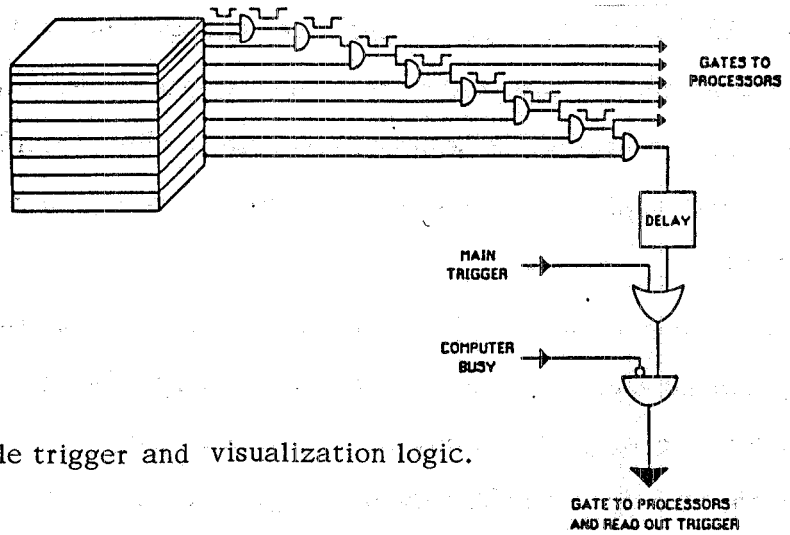

FIG. 10 - Monopole trigger and visualization logic.

In this way space information concerning hits involved in a potential trigger is transferred to processor memory and saved for subsequent readout. In order to reset the processors when a potential trigger does not reach the end of the logic chain, gates to processors also start a 20 μs 'updating' one-shot. The trailing edge of this one-shot, if in anti-coincidence with the readout 'busy' (which is immediately set by a trigger), generates a 'clear' to processors (see Fig. 11).

The monopole trigger frequency, under normal operating conditions, when triggers due to cosmic muons are subtracted, is about 3×10^{-5} Hz.

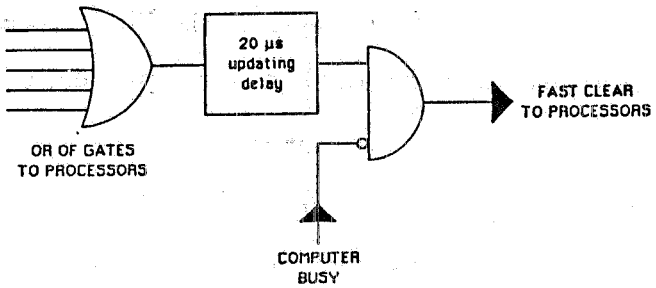

FIG. 11 - Clear logic for processors.

4. - DETECTOR PERFORMANCE

4.1. - Introduction

Fig. 12 shows a typical contained event, as represented by the event display computer program. All the basic information is displayed: the two views are pre-

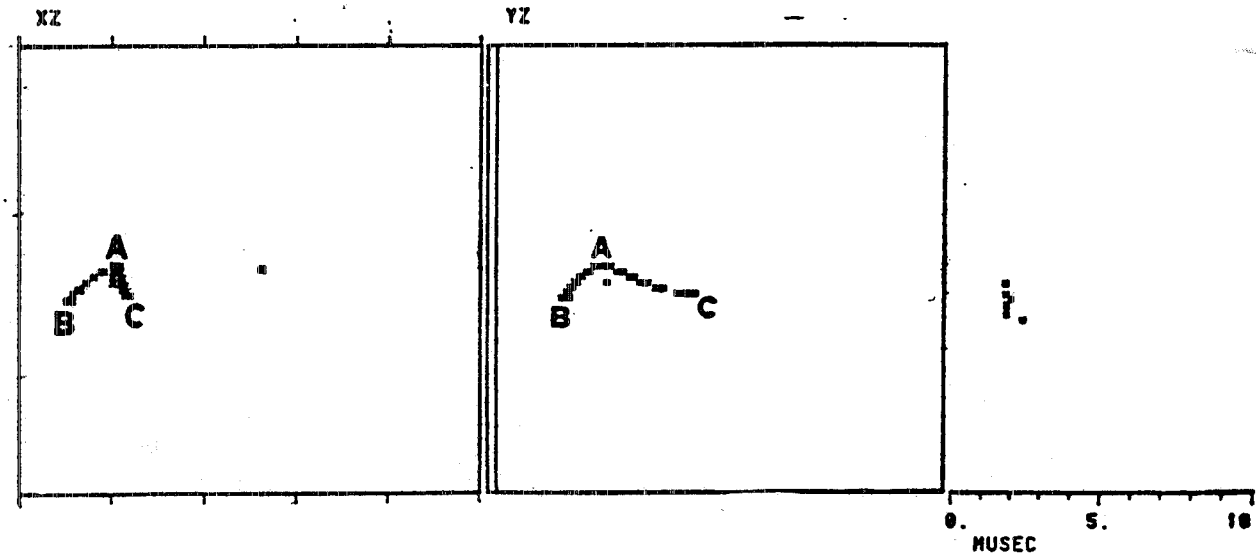

FIG. 12 - A two-prong contained event.

sented together with the timing from the OR-signals from the tube planes (100 ns resolution). It can be noticed that, due to the different characteristics of individual tracks, such as penetration, multiple hits, etc., a non ambiguous reconstruction in space is generally possible. The two-dimensional readout for each tube plane is essential in this respect.

In the following paragraphs we shall discuss space and time resolution for charged particle tracks, detection and triggering efficiency, capability of recognition track flight direction, energy resolution, π/e rejection, and directionality for e.m. showers.

4.2. - Detection Efficiency

Fig. 13 shows the average detection efficiency for a single tube plane, as measured for through-going muons, as a function of the angle of incidence. No corrections have been introduced to take into account the dead zones such as the separation of the tube modules, iron spacers, wire supports, disconnected wires, etc. The geometrical efficiency for orthogonal incidence is $\sim$ 84 % . The obtained result is in good agreement with the expectation, thus confirming that detection efficiency for the active cell of a single tube is practically 100%.

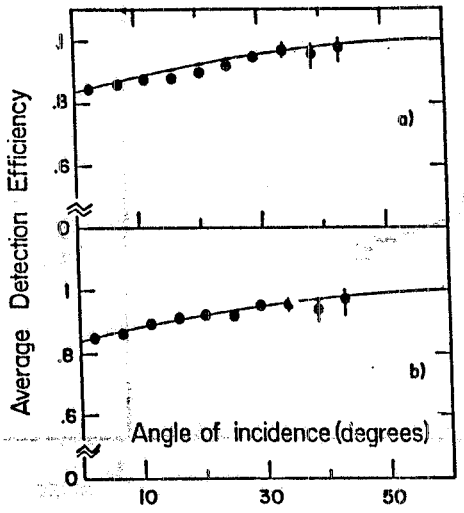

FIG. 13 - Average detection efficiency of a tube plane as a function of zenith angle. a: X-view; b: Y-view.

4.3. - Trigger and Selection Efficiency

The trigger rate is ~ 170 day^{-1} $(2 \times 10^{-3} Hz)$. About 26 triggers per day are due to cosmic muons the rest is due to rock and iron radioactivity. Atmospheric neutrinos produce about 1 trigger per month. The detector acceptance for slowly moving penetrating particles (magnetic monopoles) depends simultaneously on β and on the ionization; as shown in Fig. 14 it has a threshold at $\beta = 0.95 \times 10^{-4}$, and saturates with a value of ~ 19 m$^2 \times$sr for $\beta > 2 \times 10^{-4}$ and $I > 3 \times 10^{-2} I_{min}$.

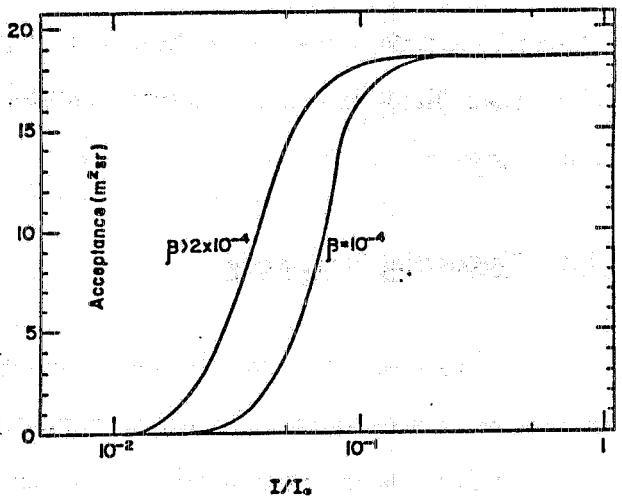

FIG. 14 - Detector acceptance for slow particles as a function of β and ionization. I_{min} is the ionization of a classical minimum ionizing particle.

Trigger efficiencies for ν_μ, $\overline{\nu}_\mu$, ν_e, $\overline{\nu}_e$, interactions inside the detector are shown in Figg. 15a-15d. Efficiencies reported in Figg. 15 are due to trigger only. In the data analysis detection efficiency is further reduced by cuts. For example, in

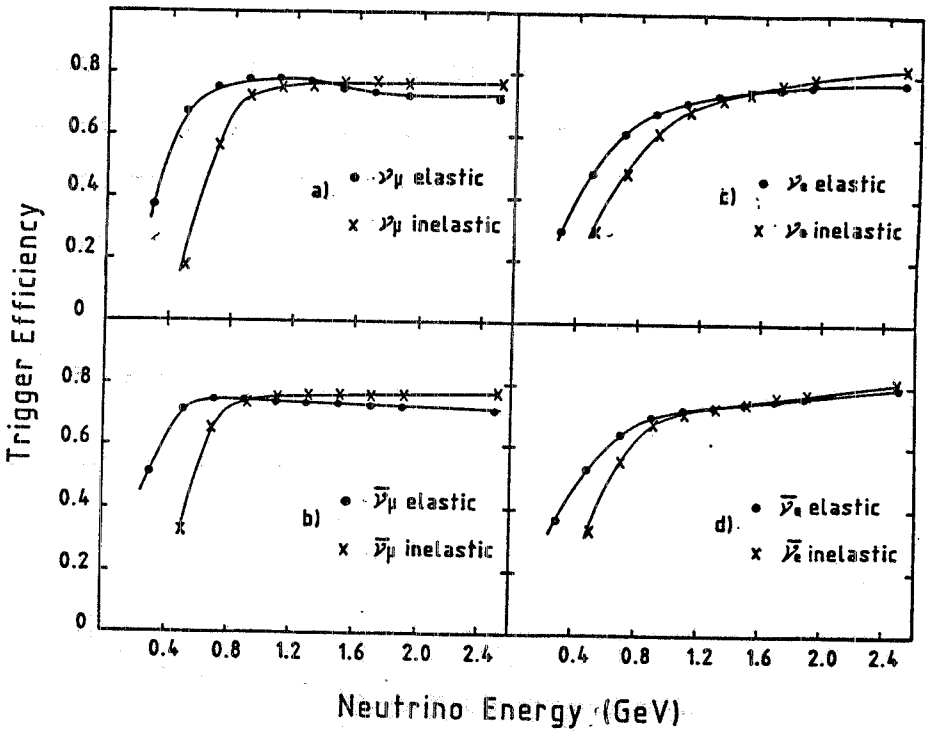

FIG. 15 - Trigger efficiencies for neutrino interactions averaged over neutrino direction, as a function of neutrino energy.

order to reject incoming particles interacting and stopping in the detector, the 'full containment' of the event is usually requested. This request has a relevant effect on high energy ν_μ events: the trigger and containment efficiency is in fact $\sim 58\%$ for a 1 GeV inelastic ν_μ interaction and falls to $\sim 26\%$ for a 2 GeV inelastic ν_μ. The trigger efficiency for nucleon decay is in the range 65%–75% (decreasing to 55%–65% for trigger and containment) for decay channels with no energetic neutrino in the final state. It has to be stressed that trigger inefficiencies are due to events hitting very few planes. In these cases however energy resolution and tracking capability would be completely lost and the event would be discarded. Trigger is then fully efficient on 'useful' events.

4.4. - Space Resolution for Charged Tracks

Space accuracy on both views has been evaluated by fitting to a straight line the high energy cosmic muon tracks. By taking the geometrical center of the cluster of hit strips, single track point resolution turns out to be ~ 3 mm on X view and

$\sim$ 3.7 mm on Y view. Average hit multiplicity is different in the two views, and depends on the track angle with respect to the wires, as shown in fig. 16 a) and b).

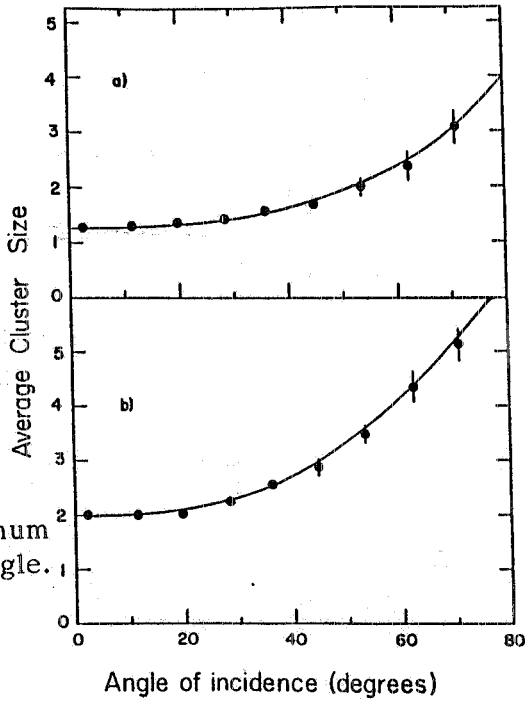

FIG. 16 - Average multiplicity for a minimum ionizing particle as function of zenith angle. a: X-view; b: Yview.

The reason of the angular dependence comes from the production of multi-streamer pulses by inclined tracks [9]. Multiplicity in the Y view is higher than for the X view, at fixed angle [5].

The angular resolution for crossing muons is dominated by multiple scattering in the rock and geomagnetic deflection. Such effects have been evaluated by measuring the parallelism of muon pairs in multiple muon events [10]; the r.m.s. angular deflection is $\sim 0.5\ ^{\circ}$. Systematic uncertainities due to possible distortion of the apparatus are negligible.

Two parallel tracks are distinguished if their separation is $\gtrsim$ 1.5 cm for orthogonal incidence.

4.5. - Timing Resolution

Track AB of Fig. 12 shows a delay of $\sim$ 300 ns in the last plane hit, with respect to the rest of the event. This delay can be considered significant at 96% c.l.. This is deduced from the time distribution of the OR signals from the tube planes, shown in Fig. 17, as measured for through-going muons.

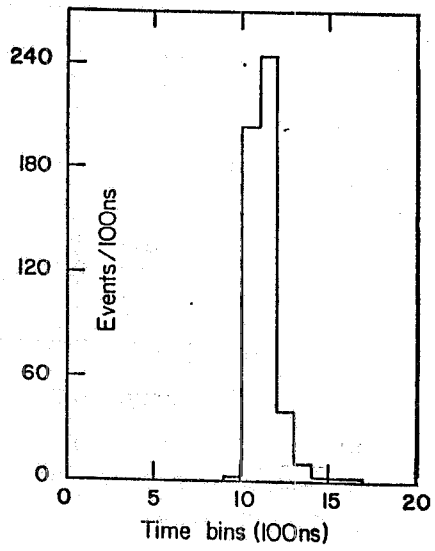

FIG. 17 - Distribution of the arrival time of the OR from planes (first hit for each plane) for a crossing muon.

The probability of detecting μ-decay is $\sim$ 35% as estimated by Montecarlo calculations. We can identify only the electrons emitted in the forward direction. Since μ^- have about 90% average probability to undergo nuclear capture in the detector material, the decay signature enables us to identify μ^+ at 95% c.l., for an equal charge flux.

The resolution of the TDCs designed to identify slow particles is monitored by means of the through-going muons, it turns out to be $\approx$ 500 ns.

4.6. - Track Shower Separation

We have developed an algorithm to discriminate shower patterns from tracks, on the basis of the results of a beam test with electrons and pions, at CERN-PS [11]. The separation criterion is based on two parameters. The first one measures the hit concentration along a path centered on the developement axis of the prong. This parameter is defined as the ratio of the number of hits inside the path with

respect to those outside. The analysis is stopped at the first visible interaction.

The second parameter is simply the sum of the number of clusters with multiplicity greater than a given threshold, each one weighted with its multiplicity. Both the road width (2 cm) and the multiplicity threshold (4) have been chosen by optimizing the efficiency of the method together with the rejection capability. Figg. 18

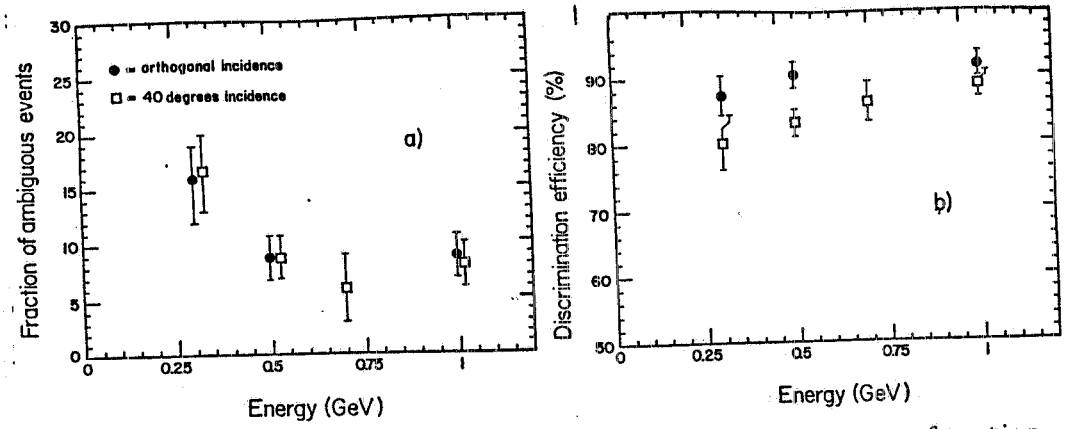

FIG. 18 - a: fraction of undistinguishable e-π events as a function of energy; b: e-π discrimination efficiency for equal electron and pion abundaces.

a) and b) show the fraction of the events for which this method gives an ambiguous response, and, on the remaining sample, the fraction of events correctly identified, as a function of the energy, for an equal abundance of particles of the different kinds. The confidence level on the information about the nature of a single event is a function of the value of the two parameters. The uncertainty is determined by the statistical fluctuation of the analyzed sample. Results are summarized in Table 1.

TABLE I - Confidence level and efficiency to discriminate electrons and pions.

Energy (MeV)	Angle of incidence (degrees)	c.l. (%) e	c.l. (%) π	Eff. (%)
300-700	0	89	86	89
300-700	40	90	92	84
1000	0	92	90	92
1000	40	94	90	89

We would like to point out that the detector structure is not optimized for e/π separation. A Pb absorber would have produced event topologies easier to disciminate, but it would have not fitted the general requirements for a proton decay experiment.

4.7. - Track Flight Direction recognition

The possible methods of identifying flight direction of tracks in our apparatus are the following:

1) μ^+-decay detection, discussed in the above paragraph.

2) Analysis of the progressive multiple scattering angle along the track.

The method adopted to analize multiple scattering is described in [12] and is based on the progressive increase of the scattering angle for decelerating particles. For every track, two fits are performed according to the two flight directions. Energy losses, Molière distribution and detector geometry have to be taken into account. The difference:

$$D = \chi^2_{correct} - \chi^2_{wrong}$$

is sensitive to the flight direction. Fig. 19 shows the efficiency for identifying the

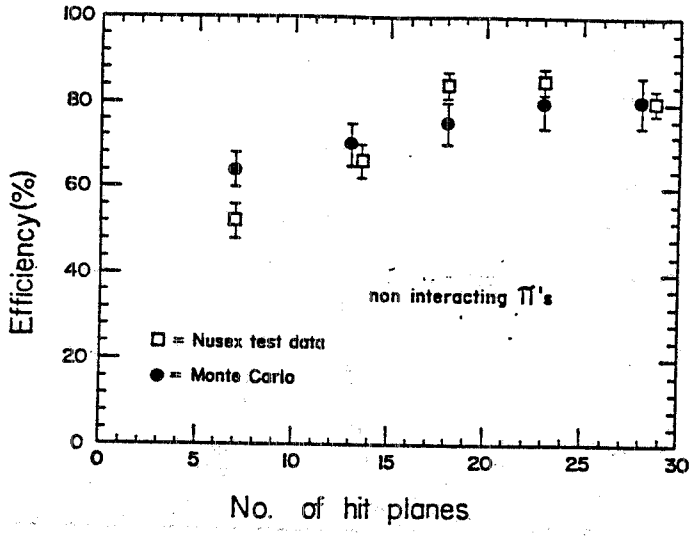

FIG. 19 - Flight direction recognition efficiency for μ-like particles as a function of particle penetration.

correct flight direction as a function of the particle penetration in the apparatus (normal incidence). Data have been taken from the beam test with π^-. We have chosen "muon-like" events, i.e. pions stopping at the end of their range, without any appreciable nuclear interaction. Montecarlo simulation is also shown. The agreement between data and Montecarlo is good and allows us to extrapolate to muons. The result is shown in Fig. 20.

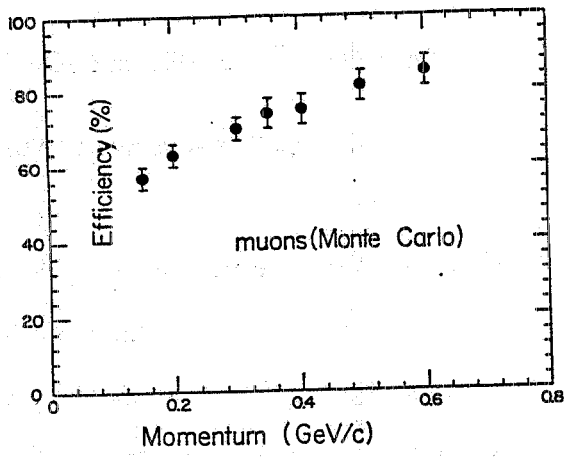

FIG. 20 - Monte Carlo evaluation of flight direction recognition efficiency as a function of muon momentum.

4.8. - Angular Resolution and Direction Recognition for e.m. Showers

Fig. 21 shows the distribution of the reconstructed angle of incidence for a sample of 500 MeV/c electrons. The axis of the shower is determined by a linear

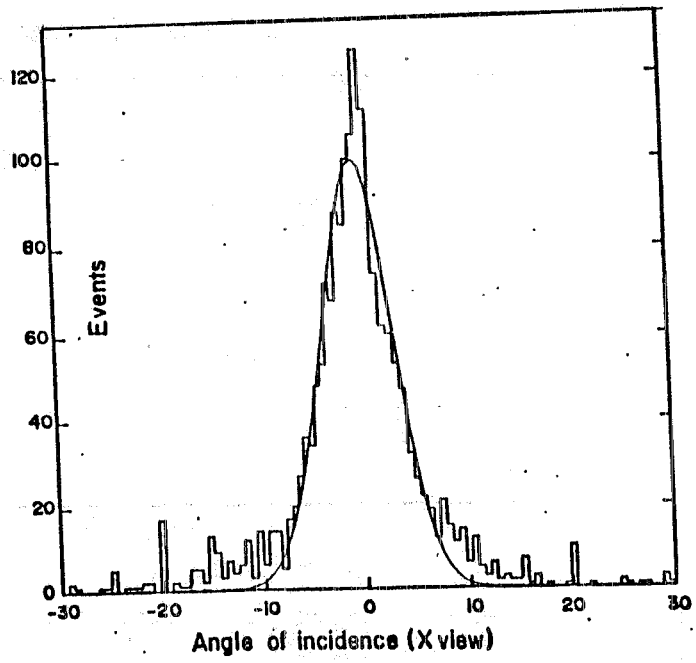

FIG. 21 - Distribution of reconstructed angle of incidence for 500 MeV electrons at normal incidence.

fit, using the centroids of the cluster of the hit strips. A selection is applied in order not to include the hits due to the conversion of soft photons, i.e. those appearing far from the event axis. The obtained angular resolution varies between 4^0 and 6^0, according to the angle of incidence.

The parameters to be used in the determination of the shower direction are:

1) the shape of the shower pattern, whose width increases with penetration;

2) the presence of gaps in the pattern, which are generally concentrated at the end of the shower, due to low energy photons, produced at the end of the e.m. cascade.

The second parameter is significant owing to the full efficiency of single tubes.

Table 2 summarizes the results concerning the efficiency and the confidence level in the recognition of the direction of showers.

TABLE II - Confidence level and efficiency to identify the direction of showers

Energy (MeV)	Angle of incidence (degrees)	Efficiency (%)	Confidence level (%)
300	0	91 ± 2	87 ± 2
300	40	85 ± 2	80 ± 2
500	0	93 ± 2	92 ± 2
500	40	86 ± 2	89 ± 2
700	40	89 ± 3	92 ± 3
1000	0	93 ± 2	92 ± 3
1000	40	87 ± 2	84 ± 2

4.9. - Energy Resolution

In a digital calorimeter, at low energy, the number of hit tubes is proportional to the energy released in the shower. The main results have been already discussed in [11]. Fig. 22 shows the measured response and energy resolution as a function of the electron energy. The over all energy resolution for a proton decay event into $e^+\pi^0$ is ~ 15 %.

The energy of π's and μ's is obtained by the measured range of the particles. The error for μ's comes from the straggling and from the discrete sampling of the track. For 500 MeV/c μ's, the sampling error becomes comparable to that due to the straggling, i.e. $\sim 3\%$ of the total range.

The situation is different for pions, which in a large fraction of cases undergo interactions with no visible energy release. This allows to give a lower limit for their energy, if only the range is considered. Fig. 23 shows the measured range distribution for 300 and 500 MeV/c π^-. At 500 MeV/c $\sim 25\%$ of pions are absorbed after 20 % of the e.m. range.

As a consequence, for two body N-decay candidate events (of the kind $e\pi$, $\mu\pi$, etc.) we require that the possible pion should have a range greater or equal to one half of the expected maximum range.

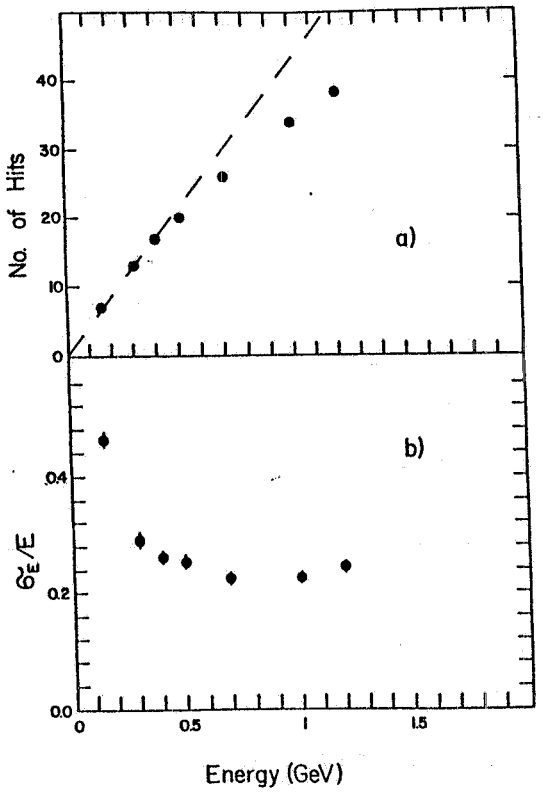

FIG. 22 - Hit response (a), and energy resolution (b), as a function of electron energy at normal incidence.

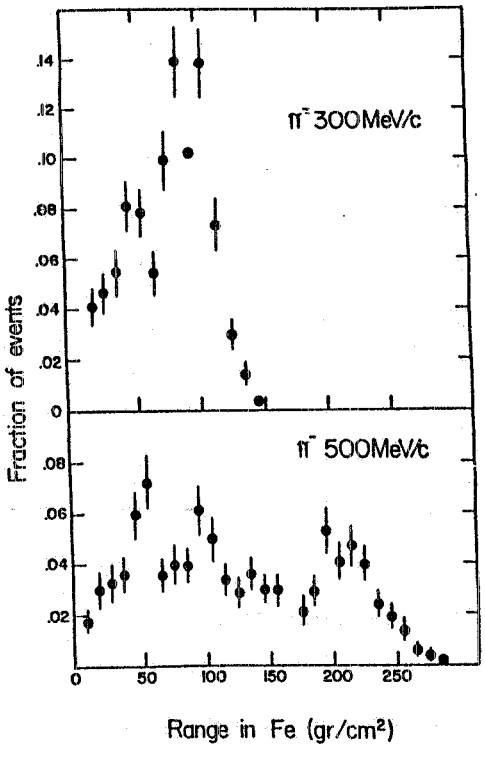

FIG. 23 - Measured range distribution for 300 MeV/c (a) and 500 MeV/c (b) π^-.

5. - DETECTOR MONITORING

The average live to total time ratio is $\sim 85\%$. The main monitoring control to check detector operation concerns the stability of the gas mixture. This is achieved by means of a test tube module inserted in one of the gas flow lines. The singles rate plateau is measured periodically, using an uncollimated β source in fixed position (see Fig. 6). Possible drifts in the relative fractions of gas components reflect in the position of the knee of the plateau. Fluctuations within $\pm$ 50 V are tolerated.

Tube operation is also monitored by the singles counting rate of the OR-signals of the tube planes, and by the total drawn current. Fig. 24 shows the total detector

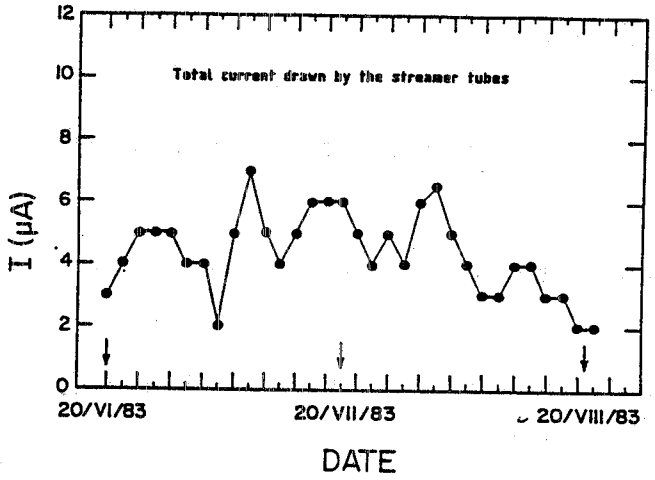

FIG. 24 - Total absorbed current as a function of time for NUSEX streamer tubes.

current as a function of time, for an observation period of two months; the average current is $\sim 6\ \mu$A. The drawn current is due to air humidity flowing through small gas leakages on some plane, whose effects concentrate at the end of the gas flow series. Recently by increasing the gas flow rate on a few planes the total average current has been brought down to 2 - 3 μA.

Further offline tube and readout monitoring is obtained by hit mapping. Fig. 25 shows the hit maps in the two views of one internal detector plane. The rising counts at the edges are due to the rock radioactivity.

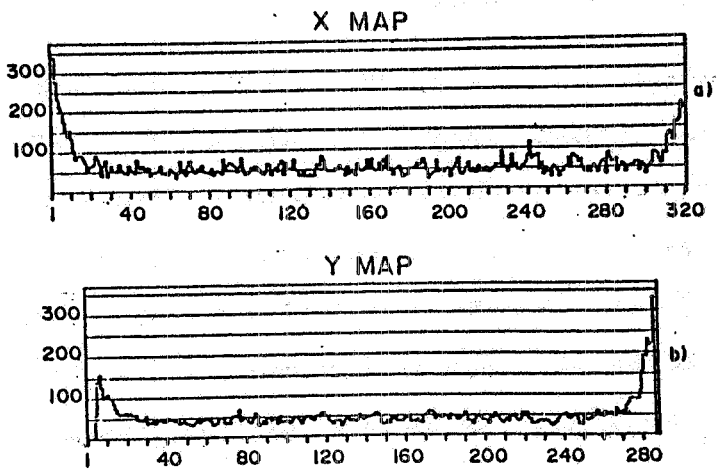

FIG. 25 - Hit map for X and Y strips for an internal detector plane.

Overall detection and triggering efficiency is monitored by the rate of the minimum trigger events.

Off-line monitoring of the detection efficiency is obtained by the analysis of the cosmic muons.

The reliability of streamer tubes has turned out to be very high. In 3 years of operation, only 20 wires went out of operation, most of them in the first two months of operation. Due to their low number (20/5000), the bad tube modules have not been substituted but simply disconnected from the high voltage. Moreover, tube performance has shown a good stability: no appreciable sign of ageing has been found. In particular, the measured average efficiency has remained at the expected level for the all observation period.

AKNOWLEDGMENTS

We wish to thank the CERN EF division for its support and particularly A. Dalluge, M. Jeanrenaud for their important contribution to the streamer tube assembly.

Thanks are due to H. Rigoni for having developed and installed the gas system.

A particular mention is due to R. Bertoni, M. Canonico, F. Chignoli, U. Denni, A. Giuliano, R. Leoni, G. Mazzenga, F. Panzeri, G.P. Pirali, O. Piolatto, G. Sala and P.P. Sverzellati for their contribution to detector installation and their skill in operating it.

Thanks are also due to the Technical Division of LNF for the continuous assistance, and in particular R. Bonini, A. Catitti, A. Di Virgilio, L. Iannotti, D. Pistoni, M. Santoni, A. Tiburzi of the OFTA-Detector Service, and G. Fuga, M. Rondinelli of the Electrotechnical Service.

Finally we would like to express our gratitude to the Direction de Expoitation Tunnel Routier sous le Mont Blanc, and to the Società del traforo del Monte Bianco, and particularly to their directors J. Louveau, F. Cuaz, and A. Porta, for help and understanding during the installation and running of the experiment.

APPENDIX A: THE MAIN TRIGGER LOGIC

The ORs from planes are fed into a multiplexer; a multiplexer controller analyzes the resulting string of bits corresponding to planes and outputs information concerning occuring patterns. However the time required for the analysis ranges from 0.5 to 2.5 μs according to the string complexity. This requires a first level reduction of the global single rate from the planes ($\approx 5 \times 10^4$ Hz) in order to keep the trigger dead time at a negligible level. This reduction is obtained by means of a group of programmable logic units (CAEN mod. C85), CAMAC interfaced to the computer, which receive as inputs the ORs of individual planes and output a signal whenever a coincidence, within 2 μs, occurs between two contiguous planes. This signal ('OR of doubles'—180 Hz frequency) starts the 100 ns resolution TDCs and, delayed by 200 ns to account for the jitter of streamers, starts the multiplexer controller. The multiplexer controller outputs 10 NIM signals. Outputs 1–9 make 3-bit, 2-bit, 1-bit words counting the occurencies of two and only two, three, four, five, > 5 contiguous planes hit. Output 10 is a NIM level indicating the end of the analysis. Outputs 1–9 are sent to a programmable logic unit which generates an output when at least one of the trigger patterns occurs. The coincidence between the stretched output of this logic unit, the OR of doubles delayed by 5 μs and the read-out anti-BUSY generates a trigger to the processors and triggers the read-out. In this way space and time information of hits occurring within 5 μs from the triggering pattern is recorded.

APPENDIX B: THE MONOPOLE TRIGGER LOGIC

We used as logic elements for the whole chain four dual 4-in 4-out programmable logic units (CAEN mod. N81). Taking as an example a downward going monopole, the trigger develops as follows: if a hit is recoded in the first group of eight planes a gate G_1 is opened for a duration of 10 μs and the hit time is recorded by TDC T_1; a signal coming from the second group of eight planes during

the open time of G_1 causes the opening of a 10 μs gate G_2, the time of this signal and of all the subsequent hits within G_1 is recorded by TDC T_2. Then a signal coming from the next block, now of 16 planes, during G_2 causes the opening of a gate G_3 for the duration of 15μs. Again the arrival time of every hit within the opening of G_2 is recorded by TDCs T_3 and T_4 corresponding to the two groups of eight planes making up the block. This sequence is repeated through the next 6 blocks of 16 planes. An output from the last block constitutes a monopole trigger. A similar logic is used for an upward going monopole.

REFERECENS

[1] For a review see P. Langaker Phys. Rep. **72**, 186 (1981);
D.V. Nanopulos: Phenomenological aspects of Unified Theories- Proc. of the XXII Int. Conf. on High Energy Physics- Edited by A. Mayer and E. Wieczorek, Leipzig, 1984., vol. 2, 36.

[2] M.R. Krishnaswamy *et al.*, Proc. Int. Coll. on Baryon Non Conservation, Bombay, Pramana Suppl. 1982, 115;
R.M. Bionta *et al.*, in *Proceedings of the XVIIth Rencontre de Moriond*, edited by J. Tran Thanh Van, (Editions Frontières, Gif sur Yvette, France 1982);
K. Ikeda *et al.*, Univ. of Tokio, UTLICEPP 82-04 (1982);
R. Bartoulaud *et al.*, Proc. Int. Coll. on Baryon Non Conservation, Bombay, Pramana Suppl. 1982, 143;
For a review on proton decay experiments see D.H. Perkins CERN/EP 84-7 (1984), to appear on *Annual Review of Nuclear Science.*

[3] A.C. Tam, E.C.M. Young, Acta Phys. Acad. Sci. Hung. **29**, Suppl. 4, 307 (1970);
J.L. Osborne and E.C.M. Joung in *Cosmic Rays at the Ground Level*, edited by A. Wolfendale (Hilger, London, 1973);
L.V. Volkova, Sov. J. Nucl. Phys. **31**, 784 (1980);
T.K. Gaisser, T. Stanev, S. Bludman and H. Lee, Phys. Rev. Lett. **51**, 223 (1983);
G. Battistoni *et al.*, Nucl. Instr. Meth. **219**, 300 (1983);
T.K. Gaisser and T. Stanev in *Proceedings of the International Conference on Baryon non Conservation, Park City, Utah, January 1984*, edited by D. Cline;
T.K. Gaisser and T. Stanev in *Proceedings of the XIth International Conference on Neutrino Physics and Astrophysics at Nordkirchen near Dortmund, June 1984*, edited by K. Kleinknecht & E.A. Paschos, p. 370 (World Scientific, Singapore, 1984);
D.H. Perkins, OUNP 85/84 (1984).

[4] M.R. Krishnaswamy *et al.*, Pramana **19**, 525 (1982);
G. Battistoni *et al.*, Phys. Lett. **133B**, 454 (1983);
B.G. Cortez *et al.*, Phys. Rev. Lett. **52**, 1092 (1984);
G. Battistoni *et al.* in *Proceedings of the XIth International Conference on Neutrino Physics and Astrophysics at Nordkirchen near Dortmund, June 1984*, edited by K. Kleinknecht & E.A. Paschos, p. 350 (World Scientific, Singapore, 1984).

[5] G. Battistoni *et al.*, Nucl. Instr. Meth. **176**, 297 (1980).

[6] G. Battistoni *et al.*, Nucl. Instr. Meth. **164**, 453 (1979).

[7] G. Battistoni *et al.*, L.N.F. 84/85(p) (1984)—Submitted to Nucl. Instr. Meth.

[8] S.P. Ahlen, Rev. Mod. Phys. **52**, 121 (1980);
S.P. Ahlen, K. Kinoshita, Phys. Rev. **26D**, 2347 (1982);
D.M. Ritson, SLAC-PUB-2950 (1982);
S.D. Drell, N.M. Kroll, M.T. Muller, B.J. Parke, M.A. Rudermann, Phys. Rev. Lett. **50**, 644 (1983);
N.M. Kroll *et al.* SLAC-PUB-3281 (1984);
L. Bracci, G. Fiorentini, R. Tripiccione, Nucl. Phys. **238B**, 167 (1984);

[9] E. Iarocci, Nucl. Instr. Meth. **217**, 30 (1983).

[10] G. Bologna et al., Nuovo Cimento **8C**, 76 (1985).

[11] G. Battistoni *et al.*, Nucl. Instr. Meth. **219** , 300 (1984).

[12] G. Battistoni *et al.*, L.N.F. 84/45(p) (1984).